Synthesis, Crystal Structure, Magnetic, and Electron Paramagnetic Resonance Properties of a Spiroconjugated Biradical. Evidence for Spiroconjugation Exchange Pathway

Natia L. Frank,[†] Rodolphe Clérac,[‡] Jean-Pascal Sutter,[†] Nathalie Daro,[†] Olivier Kahn,*[,†] Claude Coulon,[‡] Michael T. Green,[§] Stéphane Golhen,[||] and Lahcène Ouahab[||]

Contribution from the Laboratoire des Sciences Moléculaires, Institut de Chimie de la Matière Condensée de Bordeaux, UPR CNRS No. 9048, 33608 Pessac, France, Centre de Recherche Paul Pascal, UPR CNRS No. 8641, 33600 Pessac, France, Laboratoire de Chimie du Solide et Inorganique Moléculaire, UMR CNRS No. 6511, Université de Rennes 1, 35042 Rennes, France, Department of Chemistry and James Franck Institute, The University of Chicago, 5735 South Ellis Avenue, Chicago, Illinois 60637, and Beckman Institute, California Institute of Technology, Pasadena, California 91125

Received August 23, 1999

Abstract: A spiroconjugated nitronyl nitroxide biradical, 6,6′-(4,4,5,5-tetramethylimidazolidine-3-oxide-1-oxyl)-3,3,3′,3′-tetramethyl-1,1′-spirobisindane (**1**), has been prepared by functionalization of a 3,3,3′,3′-tetramethyl-1,1′-spirobisindane framework followed by Ullman condensation and subsequent oxidation. The biradical crystallizes in the monoclinic space group *C*2/*c* with four molecules in the unit cell of dimensions $a = 24.861(10)$ Å, $b = 12.129(3)$ Å, and $c = 12.258(6)$ Å. X-ray analysis of a blue-plate single crystal has revealed dihedral angles of 28° between the nitronyl nitroxide moiety and aromatic ring with intramolecular through space radical−radical distances of 8.25 and 10.11 Å. In the solid state, the temperature dependence of the molar magnetic susceptibility reveals antiferromagnetic interactions. These interactions are best fit using a pair model, affording the value $J = -4.0$ cm^{-1} where J is the interaction parameter appearing in the spin Hamiltonian $H = -J\mathbf{S}_1\cdot\mathbf{S}_2$. The field dependence of the magnetization measured at 2 K is consistent with a pair model. Frozen matrix EPR spectra of biradical **1** in CH_2Cl_2 at 100 K shows a half field transition at 1700 G. Temperature dependence of the half field transition intensity has been found to be consistent with a ground singlet state and thermally accessible triplet state. The magnetic interaction observed in the solid state is also observed in solution. Thus, room-temperature solution spectra display a nine-line pattern, with hyperfine coupling to four "equivalent" nitrogen atoms and a hyperfine coupling constant $a_N = 3.8$ G. Temperature dependence of the solution EPR spectra of biradical **1** displays alternating line width effects caused by conformational dynamics in solution. This behavior has been attributed to modulation of exchange and hyperfine interactions most likely caused by rotational motion about the nitronyl nitroxide−phenyl bond. Biradical **1** therefore exists as a ground-state singlet with a thermally accessible triplet at ca. 4 cm^{-1} higher in energy with a conformational dependence of intramolecular exchange in solution. This coupling may present evidence for spiroconjugation as an exchange pathway. Density functional calculations (B3/6-311G(D)) have been performed to investigate this possibility.

Introduction

In recent years, the design of molecular materials has involved characterization of the structure and magnetic properties of compounds containing organic radicals and coupled paramagnetic metal ions.[1−8] Among organic radicals, nitronyl nitroxides are remarkably stable because of their delocalized structure and have been extensively used in the design of molecular magnets, allowing both antiferromagnetic and ferromagnetic intermolecular interactions in the solid state.[9−14] Recent designs involve the incorporation of nitronyl nitroxide biradicals into magnetic materials with the hope of obtaining higher dimensional

[†] Institut de Chimie de la Matière Condensée de Bordeaux.
[‡] Centre de Recherche Paul Pascal.
[§] University of Chicago. Current address: Beckman Institute, California Institute of Technology, Pasadena CA 91125.
[||] Université de Rennes.

(1) Kahn, O. *Magnetism: A Supramolecular Function*; Kluwer Academic Publishers: The Netherlands, 1996.
(2) Fegy, K.; Sanz, N.; Luneau, D.; Belorizky, E.; Rey, P. *Inorg. Chem.* **1998**, *37*, 4518−4523.
(3) Handa, M.; Sayama, Y.; Mikuriya, M.; Nukada, R.; Hiromitsu, I.; Kasuga, K. *Bull. Chem. Soc. Jpn.* **1998**, *71*, 119−125.
(4) Iwamura, H.; Inoue, K.; Koga, N.; Hayamizu, T. *Assemblage of Organic Polyradicals with the Aid of Magnetic Metal Ions and Ordering of Their Spins in Macroscopic Scales*; Kahn, O., Ed.; Kluwer Academic Publishers: The Netherlands, 1996; pp 157−179.
(5) Izuoka, A.; Kumai, R.; Sugawara, T. *Adv. Mater.* **1995**, *7*, 672−674.
(6) Tanaka, M.; Matsuda, K.; Itoh, T.; Iwamura, H. *Angew. Chem., Int. Ed. Engl.* **1998**, *37*, 810−811.
(7) Miller, J. S.; Epstein, A. J. *Angew. Chem., Int. Ed. Engl.* **1994**, *33*, 385.
(8) Caneschi, A. G. D.; Sessoli, R.; Rey, P. *Acc. Chem. Res.* **1989**, *22*, 392.
(9) Caneschi, A.; Chiesi, P.; David, L.; Ferraro, F.; Gatteschi, D.; Sessoli, R. *Inorg. Chem.* **1993**, *32*, 1445−1453.
(10) Lee, C.-J.; Huang, C.-H.; Wei, H.-H.; Liu, Y.-H.; Lee, G.-H.; Wang, Y. *J. Chem. Soc., Dalton Trans.* **1998**, 171−176.
(11) Luneau, D.; Romero, F. M.; Ziessel, R. *Inorg. Chem.* **1998**, *37*, 5078−5087.
(12) Zeissel, R. *Mol. Cryst. Liq. Cryst.* **1995**, *273*, 101−110.

10.1021/ja993071a CCC: $19.00
Published on Web 02/17/2000

molecular magnets.[9,15−17] Central to such designs is the understanding of intramolecular interaction mechanisms in nitronyl nitroxide biradicals. In alkenyl and aryl conjugated biradical derivatives, antiferromagnetic interactions are often observed in which spin polarization via the carbon π orbitals well describes the observed coupling.[18,19] In some cases heteroatom substitution in conjugated biradicals highlights the interplay between spin polarization and spin delocalization that exists in biradicals. Thus, while it has been firmly established that the bridge plays a crucial role in promoting magnetic interaction,[20−25] examinations into the dependence of this interaction on conformation and substitution are sorely needed.

In the development of novel bridged biradicals, two fundamental questions must be addressed. (i) How does a particular bridge in a biradical mediate a magnetic interaction? (ii) To what extent does conformational gating of magnetic interaction perturb the system? Investigations into the effects of orientation, distance dependence, electronic coupling medium, and conformational dynamics on magnetic interaction between nitroxide moieties are thus needed. We have designed a spiroconjugated biradical **1** in which one can begin to address such questions.

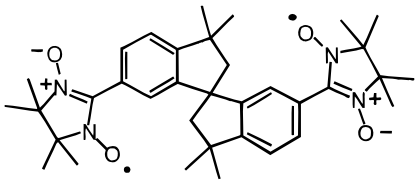

1

Spirobiradical **1** offers the ability to probe (i) the effect of nitronyl nitroxide rotational barriers (atropisomerism) on exchange pathways, through a nonconjugated phenyl linkage, and (ii) the ability of a spiroconjugated carbon to act as a pathway for magnetic interactions in the absence of classical conjugation. We herein discuss the behavior of a spiroconjugated bisnitronyl nitroxide (**1**) in which direct evidence for intramolecular and conformationally dependent magnetic interaction is observed.

Results and Discussion

Synthesis. The design of biradical **1** requires functionalization of a rigid spirocyclic framework in which the radical moieties have minimum conformational mobility with respect to the central bridge. In general, however, the syntheses of spirocyclic hydrocarbons are difficult, often involving many-step syntheses with low overall yield. Although the acid-catalyzed cyclization of phenol derivatives has made spirobisphenols synthetically accessible,[26] the functionalization of these spirocyclics has not been investigated. We herein describe an efficient route for the syntheses of functionalized spirobiindanes in which metal-catalyzed coupling allows the formation of cyano derivatives useful toward general functionalization methods. Reduction followed by condensation chemistry leads to the desired spirobiradical **1**.

The spirobisnitronyl nitroxide **1** was synthesized (Scheme 1) by a stepwise procedure based on Ullman coupling of aldehyde derivatives with 1,1,2,2-tetramethyl-1,2-bishydroxylaminoethane.[27] Starting from commercially available 4,4′-isopropylidenediphenol (**2**), acid-catalyzed cyclization leads to spirobiindane bisphenol (**3**) in 58% yield.[26] Bisphenol **3** was then triflated using a modification of the Stille procedure[28] followed by subsequent nickel(0)-catalyzed cyanation[29] to yield spirobisnitrile **5** in 69% overall yield. Reduction under Stephen's reduction conditions led to the key synthetic intermediate bisaldehyde **6** in 94% yield. Condensation of **6** with 1,1,2,2-tetramethyl-1,2-bishydroxylaminoethane[30] in ethanol at room temperature over several days yielded the radical precursor bisamidine **7.** Sodium periodate oxidation in methanol afforded the title compound spirobisnitronyl nitroxide **1** as a mixture of oxidized products. Purification by column chromatography on silica followed by recrystallization from diethyl ether−methylene chloride gave dark-blue single crystals of biradical **1** in 26% isolated yield. The biradical is relatively stable at room temperature as evidenced by no observable change in the EPR over the course of several months.

The electronic absorption spectra of nitronyl nitroxides are generally characterized by two sets of absorption bands; a short-wavelength set attributed to radical $\pi-\pi^*$ transitions and a low-intensity long-wavelength pair attributed to the n$-\pi^*$ transitions. A comparison of the absorption spectra of spirobiradical **1** with the parent phenyl−nitronyl nitroxide (PhNIT) indicates significant perturbation of the electronic structure of the aromatic radical moiety from that of the model system. Thus, the aromatic $\pi-\pi^*$ transitions of **1** (λ_{max} in nm, ϵ in parentheses: 232 (7370), 252 (6460), 274 (8580)) display a bathochromic shift from that of the parent system (211 (10 000), 232 (7500), 238 (8640), 266 (12 850)).[27] Slight perturbation of the radical structure in **1** is evident from the bathochromic shifts of the $\pi-\pi^*$ transitions (**1**, 350 (4980), 366 (7850), vs PhNIT, 346 (9300), 362 (17 700)) coupled with the larger hypsochromic shifts in the n$-\pi^*$ transitions (**1**, 584 (470), 614 (500); PhNIT, 587 (407) and 637 (450)). In addition, significant decreases in the intensities of the $\pi-\pi^*$ transitions are observed. Although the drop in transition intensity is not obvious, the bathochromic shifts are consistent with weak conjugation between the aromatic radical moieties of spirobiradical **1**.

Structural Studies. Biradical **1** was crystallized from methylene chloride−ethyl ether to give dark-blue plates, which were subjected to room-temperature X-ray diffraction analysis. Spirobiradical **1** crystallizes in the monoclinic crystal system with

(13) Caneschi, A.; Gatteschi, D. *The Chemistry and Magnetic Properties of Metal Nitronyl Nitroxide Complexes*; Lippard, S. J., Ed.; John Wiley and Sons: New York, 1991; Vol. 39, pp 332−429.
(14) Deumal, M.; Cirujeda, J.; Veciana, J.; Kinoshita, M.; Hosokoshi, Y.; Novoa, J. J. *Chem. Phys. Lett.* **1997**, *265*, 190−199.
(15) Stroh, C.; Turek, P.; Ziessel, R. *J. Chem. Soc., Chem. Commun.* **1998**, 2337−2338.
(16) Mitsumori, T.; Inoue, K.; Koga, N.; Iwamura, H. *J. Am. Chem. Soc.* **1995**, *117*, 2467−2478.
(17) Sugano, T.; Tamura, M.; Kinoshita, M. *Synth. Met.* **1993**, *55−57*, 3305−3310.
(18) Fang, S.; Lee, M.-S.; Hrovat, D. A.; Borden, W. T. *J. Am. Chem. Soc.* **1995**, *117*, 6727−6731.
(19) Kanno, F.; Inoue, K.; Iwamura, H. *J. Am. Chem. Soc.* **1993**, *115*, 847−850.
(20) Barone, V.; di Matteo, A.; Mele, F.; Moreira, I. d. P. R.; Illas, F. *Chem. Phys. Lett.* **1999**, *302*, 240−248.
(21) Chiarelli, R.; Gambarelli, S.; Rassat, A. *Mol. Cryst. Liq. Cryst.* **1997**, *305*, 455−478.
(22) Gambarelli, S.; Jaouen, D.; Rassat, A.; Brunel, L.-C.; Chachaty, C. *J. Phys. Chem.* **1996**, *100*, 9605−9609.
(23) Yamaguchi, K.; Okumura, M.; Maki, J.; Noro, T. *Chem. Phys. Lett* **1992**, *190*, 353−360.
(24) Barone, V.; Bencini, A.; di Matteo, A. *J. Am. Chem. Soc.* **1997**, *119*, 10831−10837.
(25) Castell, O.; Caballol, R.; Subra, R.; Grand, A. *J. Phys. Chem.* **1995**, *99*, 154−157.
(26) Faler, G. R.; Lynch, J. C. Substantially Pure Spirobiindane Bisphenols and Method for Their Preparation. U.S. Patent 4,791,234, 1988.
(27) Ullman, E. F.; Osiecki, J. H.; Boocock, D. G. B.; Darcy, R. *J. Am. Chem. Soc.* **1972**, *94*, 7049−7059.
(28) Echavarren, A. M.; Stille, J. K. *J. Am. Chem. Soc.* **1987**, *109*, 5478−5486.
(29) Takagi, K.; Sakakibara, T. *Chem. Lett.* **1989**, 1957−1958.
(30) Lamchem, M.; Mittag, T. W. *J. Chem. Soc. C* **1966**, 2300.

Scheme 1. Synthesis of Spirobiindane Biradical (**1**)[a]

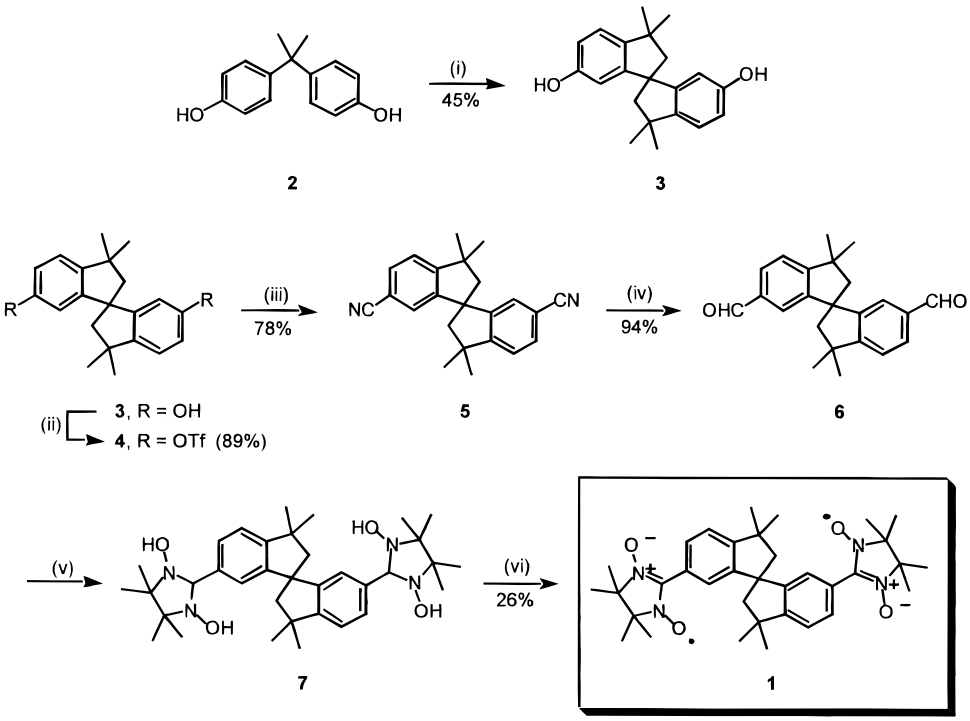

[a] Reagents and conditions: (i) methanesulfonic acid, 135 °C, 4 h; (ii) triflic anhydride (2.0 equiv), Bu_3N (2.0 equiv), CH_2Cl_2, 25 °C, 14 h; (iii) KCN (4.5 equiv), PPh_3 (0.045 equiv), $(PPh_3)_2NiBr_2$ (0.09 equiv), zinc dust (0.30 equiv), CH_3CN, 60 °C, 3.5 h; (iv) $SnCl_2 \cdot HCl$ (3.5 equiv), Et_2O, 25 °C; H_2O, 60 °C, 3 h; (v) 1,1,2,2-tetramethyl-1,2-dihydroxylaminoethane (2.0 equiv), ethanol, 30 °C, 64 h; (vi) $NaIO_4$ (0.1 equiv), methanol, 5 min.

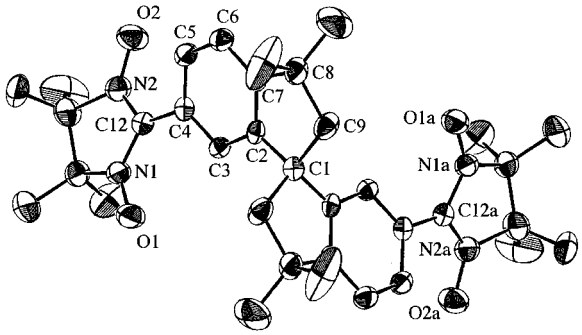

Figure 1. ORTEP diagram of spirobiindane biradical (**1**) showing 50% probability thermal ellipsoids for all nonhydrogen atoms.

space group *C*2/*c*, in which the asymmetric unit corresponds to half of the molecule. There are four stereoisomers (atropisomers) possible due to rotation about the phenyl radical carbon−carbon bond, yet the spirobiradical is centrosymmetric with a 2-fold symmetry axis through the central spirocyclic carbon C1 (Figure 1). The best-fit plane of the benzene ring makes an angle of 28.0(3)° with the radical moiety, similar to that reported for the nitronyl nitroxide radical PhNIT.[31] The nearly 30° dihedral angle suggests that the minimum energy conformation is a balance of ortho−ortho steric interactions, which would favor a dihedral angle of 45°, and delocalization between the radical moiety and aromatic ring, which would favor a planar conformation.

The nitronyl nitroxide moiety itself maintains the structural features typical of other nitronyl nitroxide derivatives.[9] In particular, the O−N−C−N−O moiety is planar, with nearly equivalent O−N bond lengths of 1.296(4) Å (N(1)−O(1)) and 1.279(3) Å (O(2)−N(2)), consistent with orbital conjugation.

(31) Wong, W.; Watkins, S. F. *J. Chem. Soc., Chem. Commun.* **1973**, 888.

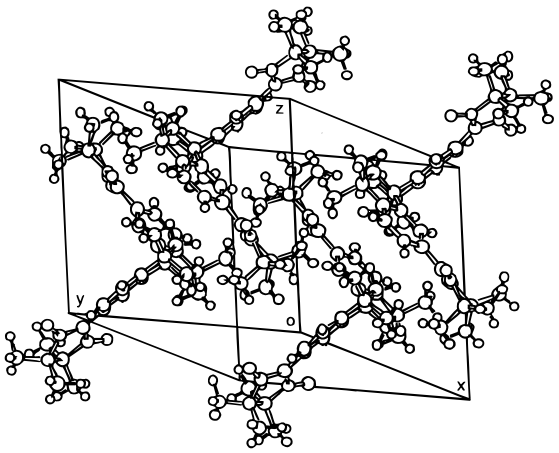

Figure 2. View of unit cell with $Z = 4$ molecules showing pair packing of enantiomers.

In addition, the methyl groups of the nitroxide moiety are in the staggered conformation, leading to partial twisting of the five-membered ring (−12.6°). An analysis of intramolecular radical··radical contacts suggests that the intramolecular through space O··O contacts in biradical **1** are too large for any significant through-space overlap of radical magnetic orbitals (8.25 Å between O(2) and O(1a), and 10.11 Å between O(1) and O(1a)).

The crystal lattice structure can be described as pairs of enantiomers forming ribbons along the *c* direction. The unit cell contains two pairs of enantiomers, each enantiomer being related to the other by a 2-fold screw axis along the *a* direction (Figure 2). The pairs of enantiomers are oriented such that the closest contacts exist between the spirobiindane methyl hydrogens and the best-fit plane of the enantiomeric aromatic ring (H···ring = 3.4 Å) and the nitroxide (H···O = 2.71 Å). No direct radical−

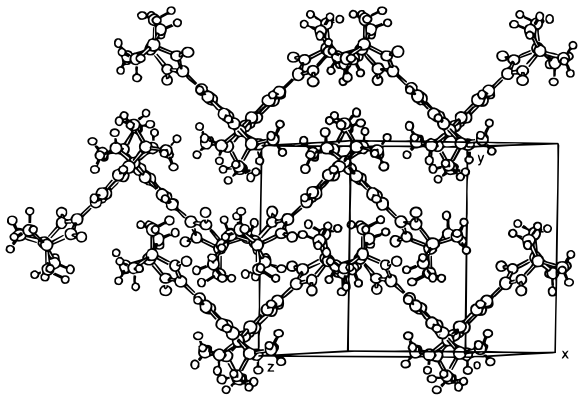

Figure 3. View of packing showing nearest-neighbor radical−radical interactions.

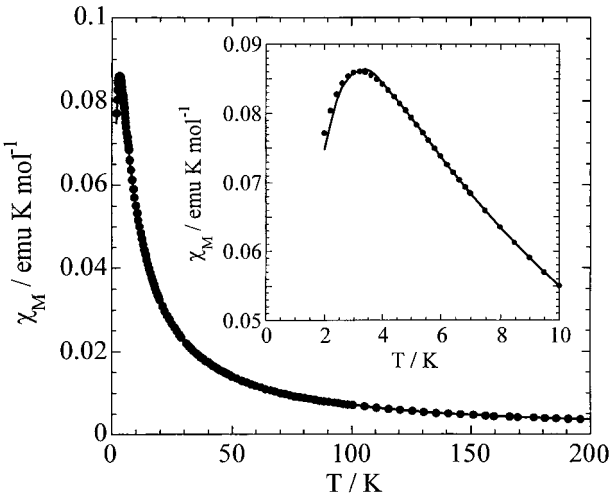

Figure 4. Experimental (●) and calculated (−) temperature dependence of the molar magnetic susceptibility for a polycrystalline sample of spirobiradical **1**. The inset zooms in on the data below 10 K.

radical intermolecular contacts are apparent between pairs of enantiomers.

A three-dimensional array consists of rows of molecules staggered by a glide plane operation, creating parallel ribbons along the *bc* direction (Figure 3). The closest intermolecular radical−radical O···O contacts between neighboring molecules occur in the *ac* plane at 4.54 Å (along the ribbon) and 6.12 Å (between ribbons). An estimation of the magnitude of through space antiferromagnetic interactions between nitronyl nitroxides can be made from distance relationships previously established.[13] In general, contacts at distances greater than 5 Å can be considered to give rise to negligible magnetic interactions, while the shortest observed contact of 4.5 Å would yield an interaction of about 0.5 cm^{-1}. Thus, analysis of the crystal structure suggests that in the solid state of spirobiradical **1**, only small intermolecular exchange interactions of about 0.5 cm^{-1} must exist between biradicals.

Solid-State Magnetic Susceptibility. The rigid carbon framework of spirobiradical **1** offers the possibility for *intramolecular* magnetic interaction of the nitronyl nitroxide moieties. Thus, to determine whether biradical **1** behaves as an exchange coupled system, the magnetization was measured as a function of temperature and field. The molar magnetic susceptibility, χ_M, of a polycrystalline sample of spirobiradical **1** was measured in the temperature (T) range 2−300 K at a field strength of 0.1 kOe. The χ_M versus T plot is shown in Figure 4. Diamagnetic corrections were calculated from the slope of a plot of $\chi_M T$ vs T in the high-temperature ($T > 100$ K) region and were found

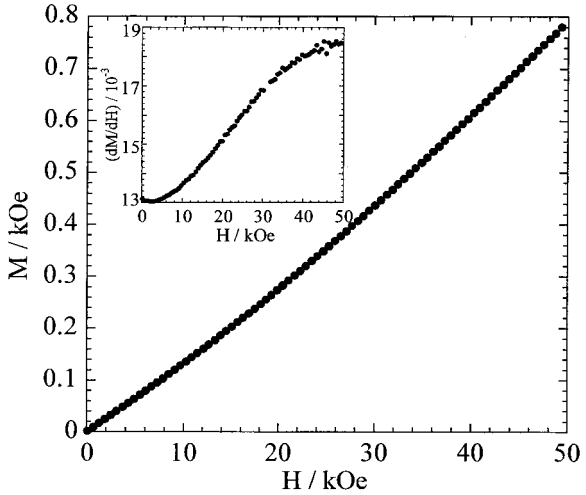

Figure 5. Experimental (●) and calculated (−) field dependence of the magnetization at 2 K for a polycrystalline sample of spirobiradical **1**. The inset shows the field dependence of the derivative (dM/dH).

to be -8.4×10^{-4} emu K mol^{-1}. The use of Pascal's tables would lead to a less negative value, -3.0×10^{-4} emu K mol^{-1}. At temperatures between 60 and 200 K, $\chi_M T$ is constant and equal to 0.70 emu K mol^{-1}, a value close to that expected for two isolated $^1/_2$ spins. As the temperature falls below 60 K, χ_M increases and reaches a maximum at 3.4 K, the signature for antiferromagnetic interactions. A Curie Weiss plot of $1/\chi$ vs T yields a Curie constant of 0.70 emu K mol^{-1} and a Weiss constant of −4.0 K (-2.8 cm^{-1}), consistent with antiferromagnetic interactions. These magnetic susceptibility data can be nicely fit to a Bleaney−Bowers expression (eq 1) for an isolated two-spin $^1/_2$ model:[32,33]

$$\chi_M = \frac{2N\beta^2 g^2}{kT\left[3 + \exp\left(\frac{-J}{kT}\right)\right]} \tag{1}$$

where β is the electronic Bohr magneton, N is Avogadro's number, g is the Zeeman factor, k is Boltzmann's constant, and J is the interaction parameter appearing in the spin Hamiltonian $H = -J\mathbf{S}_1 \cdot \mathbf{S}_2$. The fit of this expression to experimental data leads to $J = -4.0$ cm^{-1}.

Further evidence for the existence of pairs of spins in the solid state was found through magnetization vs field studies. The dependence of the magnetization M on field H for such a pair is given by[34,35]

$$M = 2Ng\beta \frac{\sinh\left(\frac{g\beta H}{kT}\right)}{\exp\left(\frac{-J}{kT}\right) + 1 + 2\cosh\left(\frac{g\beta H}{kT}\right)} \tag{2}$$

For cases in which J is negative, in the absence of a magnetic field, the ground state is a singlet. At field values below a critical value H_c, in which $H_c = -J/(g\beta)$, the magnetization increases with field because of the thermal population of the low-lying triplet excited state. As H approaches H_c, crossover between the singlet state and the $M_s = -1$ Zeeman component of the triplet state occurs, causing a maximum in the first derivative dM/dH.

(32) Bleaney, B.; Bowers, K. D. *Proc. R. Soc.* **1952**, *A214*, 451−456.
(33) Carlin, R. L. *Magnetochemistry*; Springer-Verlag: New York, 1986.
(34) Bergerat, P.; Kahn, O.; Legoll, P.; Drillon, M.; Guillot, M. *Inorg. Chem.* **1994**, *33*, 2049−2051.
(35) Kahn, O.; Launay, J. P. *Chemtronics* **1988**, *3*, 140.

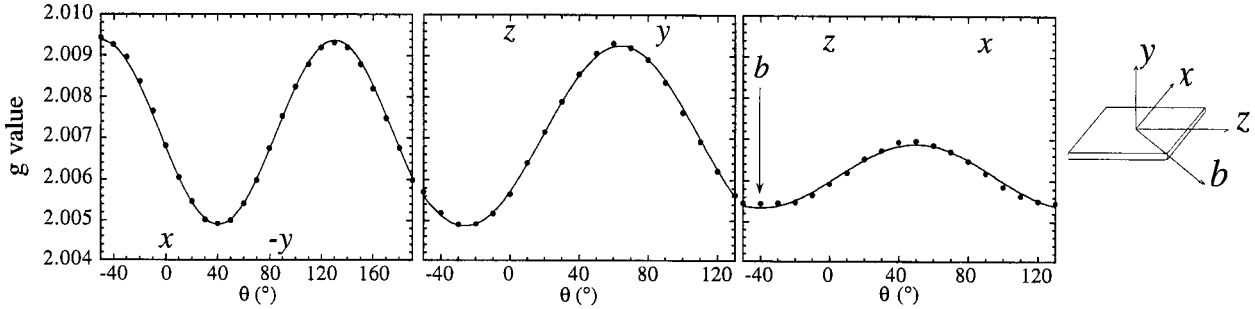

Figure 6. Angular dependence of the observed *g* values for rotation of a single crystal of **1** in the *xz*, *yz*, and *xy* planes, in which the *x*, *y*, and *z* axes correspond to the coordinate system also shown in the figure.

The field dependence of the magnetization was measured at $T = 2$ K for field strengths H up to 50 kOe (Figure 5). The M vs H curve shows an upward curvature characteristic of a singlet ground state and low-lying excited magnetic state. A plot of the first derivative of the magnetization with respect to field strength suggests a maximum just above 50 kOe (Figure 5, inset). A fit of the M vs H curve with expression 2 yielded a J value of -4.2 cm^{-1}. The accuracy of the J value deduced from this field dependence of the magnetization is lower than that deduced from the temperature dependence of the magnetic susceptibility. This is due to the fact that the population of the triplet state at 2 K is already rather important and that the transition around H_c is rather smooth.

Solid State: Single-Crystal EPR Measurements. Room-temperature single-crystal EPR spectra recorded on a single plate crystal of dimensions $1 \times 1 \times 0.3$ mm^3 at X-band frequency show a single exchange-narrowed Lorentzian line with a line width between 3.9 and 19.7 G, depending on the crystal orientation with respect to the magnetic field. If the biradicals were perfectly isolated in the monoclinic lattice, two lines should be observed, merging for some specific orientations. In fact, an averaging effect occurs. Three coordinate axes *x*, *y*, and *z* are defined for a right-handed coordinate system such that *x* and *z* are in the plane of the crystal, parallel to the crystal edges, and *y* is perpendicular to the large crystal face, as shown in Figure 6. Rotation with respect to an external field H in the *xy*, *yz*, and *xz* planes of the crystal (Figure 6) yielded the following principal values for the **g** tensor: $g = 2.013$, 2.0054, and 2.0045. As expected, one of the principal directions of the **g** tensor is aligned along the 2-fold rotation axis, *b*. The degree of *g*-factor anisotropy present in biradical **1** is consistent with those of other nitronyl nitroxide derivatives.[9]

Solid State: EPR Matrix Studies. In single crystals, the spin centers are restricted to only a few conformations because of the long-range organization of the crystal. In glassy matrices, however, only local correlation of atomic positions is possible, since a wide range of conformations may exist. Thus, the magnetic behavior observed for a conformationally mobile molecule in glassy matrices may be the sum of the contributions due to the population of possible conformers. The magnetic behavior of biradical **1** in various solvent matrices was investigated by measuring the intensity of the $\Delta M_s = 1$ transition as a function of temperature between 4 and 150 K. This intensity is proportional to the molar magnetic susceptibility. The normalized reciprocal intensity data of the $\Delta M_s = 1$ are shown in Figure 7. With only slight deviations, the $\Delta M_s = 1$ transitions in toluene, chloroform, and carbon tetrachloride behave remarkably similarly to each other and follow Curie−Weiss behaviors with Weiss constants around -4 ± 1 K (2.8 cm^{-1}), consistent with the magnetic susceptibility of a polycrystalline sample. Thus, magnetically dilute biradical **1** exhibits weak but distinct

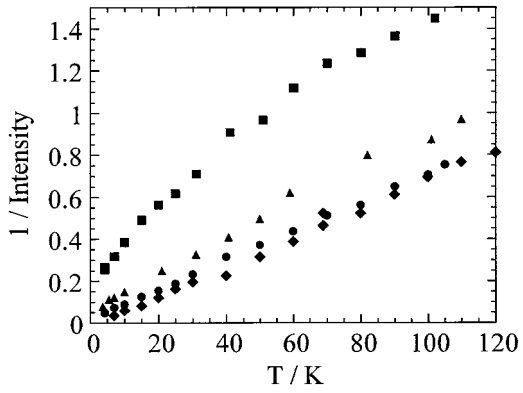

Figure 7. Temperature dependence of the reciprocal intensities of the EPR transitions ($\Delta M_s = 1$) for spirobiradical **1** in (◆) methylene chloride, (●) carbon tetrachloride, (■) chloroform, and (▲) toluene matrixes. Intensities were normalized to values at 140 K for each data set.

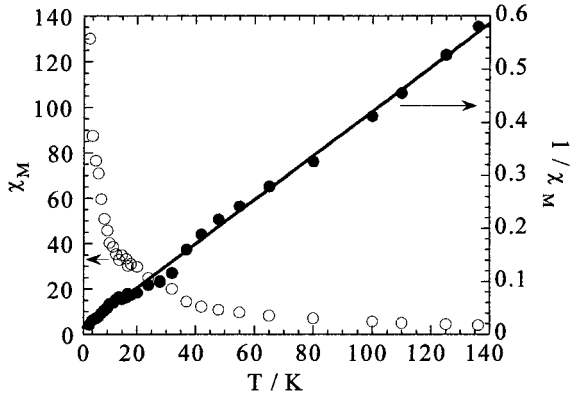

Figure 8. Temperature dependence of the normalized intensities, shown as χ_M and $1/\chi_M$, of the $\Delta M_s = 2$ transition for spirobiradical **1** in a methylene chloride matrix.

antiferromagnetic coupling, confirming that the observed antiferromagnetic coupling in the crystalline state arises from intramolecular interactions. Both the powder magnetic susceptibility measurements and EPR intensity measurements reveal that biradical **1** exists in the singlet ground state with a thermally accessible triplet state. In such a case, the relative population of the triplet state is governed by the Boltzmann distribution law.[32] The EPR absorption intensity I of the triplet state is expected to vary as a function of temperature according to eq 1. The presence of a triplet state was evidenced by the appearance of a $\Delta M_s = 2$ transition (methylene chloride, $T <$ 136 K) at a field of 1700 G. The intensity of this transition was measured as a function of temperature and is shown normalized to 136 K as I and $1/I$ (i.e., χ_M and $1/\chi_M$) vs T in Figure 8. The temperature dependence of the intensity of the $\Delta M_s = 2$

transition in the temperature range 136−4 K can be fit to expression 3, in which J is then found as -2.4 cm^{-1}.

In summary, the solid-state magnetic behavior of biradical **1** can best be fit by a pair spin $^1/_2$ model, in which antiferromagnetic coupling leads to a singlet ground state and thermally accessible triplet state, with a singlet−triplet energy gap of about $J = -4$ cm^{-1}. Crystal structure analysis suggests that this antiferromagnetic coupling cannot arise from intermolecular interactions and most likely is intramolecular in nature, occurring through the spiro framework. EPR matrix studies confirm the intramolecular nature of the interaction.

Solution State: EPR Studies. The temperature dependence of the X-band EPR spectra of biradical **1** in solution (methylene chloride) was recorded. At room temperature, the spectrum consists of a well-resolved symmetrical nine-line pattern centered at $g_{iso} = 2.0032$ with intensities close to 1:4:10:16:19:16:10:4:1 ratio, and a hyperfine coupling, $a_N = 3.75$ G. The spectrum also shows slight broadening of the right half. The intensities as well as a slight asymmetry of the spectrum are consistent with hyperfine coupling with four equivalent nitrogen nuclei and incomplete averaging of the parallel and perpendicular components. Thus, at room temperature, the biradical **1** exhibits rapid exchange coupling and is in the strong exchange regime where $|J| \gg a_N$. As the temperature of the sample is decreased, coalescence and changes in the relative intensities of the transitions are observed (see Figure 9). Line broadening and intensity loss can be seen in lines 2, 4, 6, and 8 while lines 1, 3, 5, 7, and 9 maintain intensity and line width. As the temperature approaches the melting temperature of methylene chloride, 190 K, the spectrum essentially appears as a five-line spectrum with hyperfine splitting constants of 7−8 G.

The temperature dependence of the $\Delta M_s = 1$ transition is somewhat a function of solvent viscosity and polarity. Thus, in toluene, chloroform, and carbon tetrachloride, the EPR spectra at 295 K also display a nine-line pattern, with slight variation in relative intensities and line widths from that observed in methylene chloride. The temperature dependence of these spectra are qualitatively maintained in all of the solvents examined. Thus, the slight variations in the coalescence temperatures and the nature of line width effects are consistent with differences in melting temperature and viscosity within the series. At temperatures far below the melting point, for instance 114 K, one observes complete coalescence into one broad line 125 G in width. X-band EPR spectrum of a powder sample of spirobiradical **1** at room temperature also gives a simple single line (Zeeman factor $g = 2.0032$) with broadening due to zero-field splitting (115 G width). Thus, the low-temperature spectrum is essentially that of the powder spectrum.

In an isotropic phase with unaveraged zero-field splittings, the spin Hamiltonian for a biradical interacting with nuclear spins (noted I_1 and I_2), and allowing for exchange interactions, is[36]

$$\mathbf{H} = g_{av}\beta H(\mathbf{S}_{1z} + \mathbf{S}_{2z}) + a_{av}(\mathbf{I}_{1z}\mathbf{S}_{1z} + \mathbf{I}_{2z}\mathbf{S}_{2z}) - J_{av}\mathbf{S}_1\cdot\mathbf{S}_2 \quad (3)$$

where g_{av}, a_{av}, and J_{av} are averaged values. We presently interpret the solution spectra in terms of Zeeman and hyperfine exchange interactions in which the dipolar interaction contributes only to the relaxation, leading to an overall increase in the line width of the absorptions. Thermal effects on EPR spectral line shapes may be due to two distinct types of line-broadening mechanisms: (i) general line width broadening due to intermolecular electron spin exchange, electron transfer, proton transfer, or fluxional motion; (ii) line width variation due to dynamic hyperfine contributions, in which variation in line width with M_i is observed.[37−40] Variations in line widths become evident upon decreasing temperature and may be due to either in-phase or out-of-phase dynamic modulation of hyperfine splitting. In the case of in-phase modulations, the nuclei *a* and *b* are instantaneously equivalent, and hyperfine splittings, a_a and a_b, increase or decrease (are modulated) in unison. Thus, the nuclei are instantaneously and dynamically equivalent. In this case, line widths vary as M_I^2. When the two sets of nuclei *a* and *b* are inequivalent, out-of-phase modulation of hyperfine splittings leads to an interchanging and therefore averaging of hyperfine splittings. Such an effect is termed alternating line width effect and leads to the dynamic equivalence of nuclei *a* and *b*; the line widths vary as $M_I = \pm 1$.[41,42]

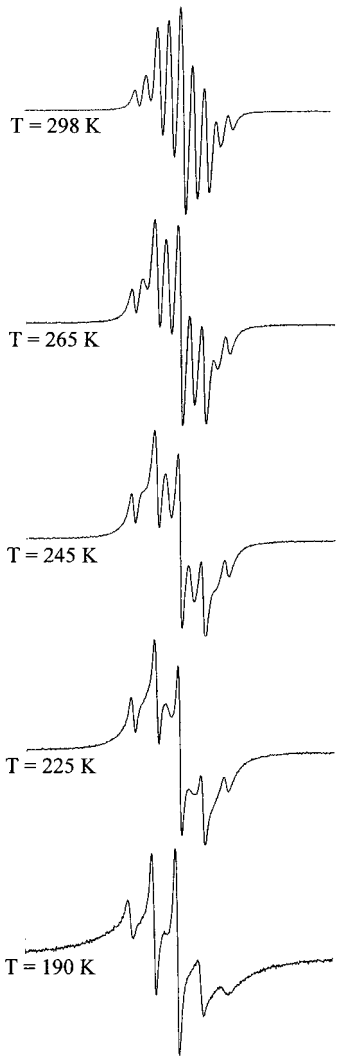

Figure 9. EPR spectra of spirobiradical **1** in methylene chloride at some selected temperatures.

Analysis of the spectra from 190 to 245 K indicates that the nine-line pattern is effectively maintained as the temperature decreases. However, the severe loss of intensity and line width

(36) Falle, H. R.; Luckhurst, G. R.; Lemaire, H.; Marechal, Y.; Rassat, A.; Rey, P. *Mol. Phys.* **1966**, *11*, 49−56.

(37) Fraenkel, G. K. *J. Phys. Chem.* **1967**, *71*, 139−171.
(38) Kivelson, D. *J. Chem. Phys.* **1960**, *33*, 1094.
(39) McLachlan, A. D. *Proc. R. Soc. A* **1964**, 271.
(40) Luckhurst, G. R. *Biradicals as Spin Probes*; Berliner, L. J., Ed.; Academic Press: New York, 1976; pp 133−181.
(41) Bolton, J. R.; Carrington, A. *Mol. Phys.* **1962**, *5*, 161−167.
(42) Freed, J. H.; Fraenkel, G. K. *J. Chem. Phys.* **1962**, *37*, 1156−1157.

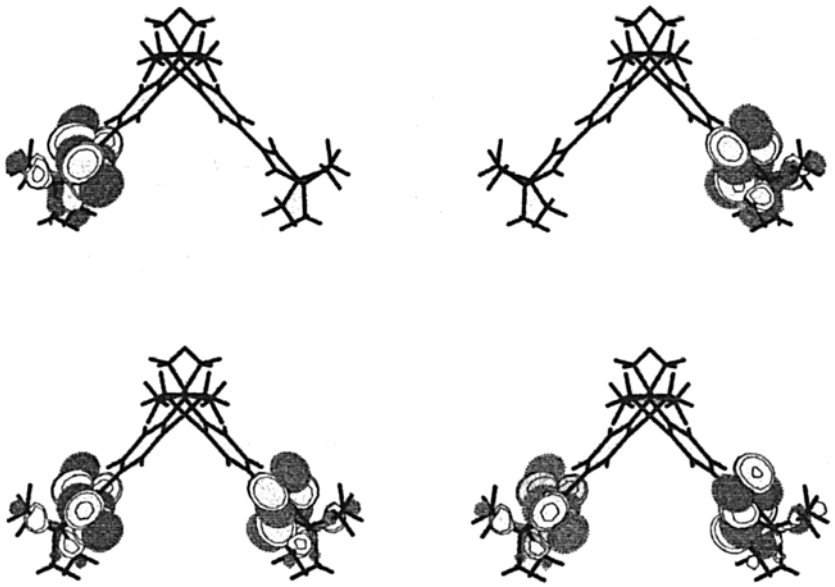

Figure 10. (a, top) α-Spin and β-spin orbitals for the unrestricted singlet and (b, bottom) α-spin and β-spin orbitals for the unrestricted triplet of spirobiradical **1**. Calculations were performed at the B3LYP/6-311G(d) level. The orbitals are shown at a contour value of 0.02.

broadening in lines $M_I = \pm 1, \pm 3$ with decreasing temperature is consistent with the dynamic modulation of hyperfine coupling. Interpretation of this effect can be understood by the consideration of two sets of N nuclei with $I = 1$. It is assumed that the radical can exist in two thermodynamic states that are equal in energy. In one state, hyperfine coupling to the two nitrogen nuclei of one nitroxide moiety may be strong (a_a large) with hyperfine coupling to the other radical moiety being weak (a_b small). In the second state, the hyperfine couplings are modulated such that hyperfine coupling a_a is small and hyperfine coupling a_b is large. Interconversion rates between these two states relative to the EPR time scale dictates the appearance of the spectrum. Thus, at fast interconversion rates, the hyperfine splittings are completely averaged and a nine-line pattern (four nuclei with $I = 1$) would be observed. As the relative rates of interconversion slow, the alternate lines broaden and eventually coalesce, leading to an apparent hyperfine coupling to two nuclei with $I = 1$. Rotational isomerism about the nitronyl nitroxide−phenyl bond in spirobiradical **1** leading to dynamic equivalence would explain the hyperfine coupling to four "equivalent" nuclei that do not possess equivalent local symmetry because of the axial chirality of biradical **1**. In addition, because exchange coupling and hyperfine coupling parameters are both functions of electron and spin densities, the rotational motion that modulates hyperfine coupling would also modulate J. Thus, conformational gating of exchange and hyperfine coupling parameters would explain the temperature and solvent dependences of the EPR spectra of spirobiradical **1**.

Computation. Density functional calculations were performed on spirobiradical **1** in order to investigate both the singlet−triplet energy gap and spin density populations. By use of the crystal structure geometry, unrestricted calculations (Gaussian 94[43]) were performed at the B3LYP/6-311G(d) level. The singlet and triplet solutions were found to be degenerate ($J = 0$), consistent with the small exchange coupling parameter found by magnetic susceptibility measurements.

Table 1. Theoretical Atomic Spin Populations for the Triplet and Singlet States (HOMO, α-Spin Density) of Spirobiradical **1** at the B3LYP/6-311G(d) Level and Comparison with Phenyl Nitronyl Nitroxide (PhNIT)[44,45]

site	atomic spin populations of triplet state **1**, B3LYP/ 6-311G(d)	atomic spin population of singlet state **1**, B3LYP/ 6-311G(d)	experimental atomic spin population of PhNIT[a]	theoretical atomic spin population of PhNIT (VWN/DZVP)[a]
O1	0.339	0.339	0.247(13)	0.288
N1	0.261	0.261	0.278(16)	0.210
C12	−0.196	−0.196	−0.121(17)	−0.065
N2	0.269	0.269	0.278(15)	0.238
O2	0.342	0.342	0.277(13)	0.319
C4	0.037	0.038	0.024(16)	0.004
C3	−0.037	−0.037	0.000(13)	−0.009
C2	0.017	0.016	0.025(13)	0.002
C1	−0.002	0.000		
C9	0.000	0.000		
C8	0.002	0.002		
C7	−0.031	−0.031	−0.016(12)	−0.009
C6	0.017	0.017	0.011(12)	0.002
C5	−0.033	−0.033	−0.037(13)	−0.009

[a] Values for PhNIT are taken from Table 8 of ref 44.

The singly occupied molecular orbitals of the unrestricted singlet and triplet solutions are shown in Figure 10. The orbitals of the singlet are localized such that the up and down spin electrons occupy different sides of the molecule, which is consistent with the symmetry breaking inherent in the methodology. The triplet orbitals on the other hand are completely delocalized. The spin-squared expectation value for the singlet state is equal to 1.1, which corresponds to a significant amount of spin contamination. A wave function with $\langle S^2 \rangle = 0$ could be calculated; however, its energy would be higher than that of the triplet state.

A comparison of the spin densities for **1** with the model system phenyl nitronyl nitroxide (PhNIT) would indicate possible modulations of the spin density by the spiro framework (Table 1). The spin densities on the phenyl and ONCNO region of **1** agree qualitatively with those obtained from experimental

(43) Frisch, M. J.; Trucks, G. W.; Schlegel, H. B.; Gill, P. M. W.; Johnson, B. G.; Robb, M. A.; Cheeseman, J. R.; Keith, T.; Petersson, G. A.; Montgomery, J. A.; Raghavachari, K.; Al-Laham, M. A.; Zakrzewski, V. G.; Ortiz, J. V.; Foresman, J. B.; Cioslowski, J.; Stefanov, B. B.; Nanayakkara, A.; Challacombe, M.; Peng, C. Y.; Ayala, P. Y.; Chen, W.; Wong, M. W.; Andres, J. L.; Replogle, E. S.; Gomperts, R.; Martin, R. L.; Fox, D. J.; Binkley, J. S.; Defrees, D. J.; Baker, J.; Stewart, J. P.; Head-Gordon, M.; Gonzalez, C.; Pople, J. A. *Gaussian 94*, revision C.2; Gaussian, Inc.: Pittsburgh, PA, 1995.

and theoretical studies of PhNIT.[44] The singlet and triplet states have identical spin populations on oxygen (0.34$N\beta$), nitrogen (0.27$N\beta$), and the bridging carbon of the nitronyl nitroxide ($-0.19N\beta$).[45] The spin populations of the phenyl moiety alternate in sign, ranging in value from 0.017$N\beta$ to 0.038$N\beta$. In general, however, the magnitudes of the spin populations found for **1** are larger than those found in the PhNIT studies. By symmetry, the unrestricted singlet solution can have no spin density at the spirocarbon (C1). No such restrictions exist for the triplet, which has a small negative spin population ($-0.002N\beta$) at this position.

Conclusions

The synthesis and characterization of a novel chiral bisnitronyl nitroxide have been reported. In the solid state, magnetization measurements vs temperature and field are consistent with a ground-state singlet and a low-lying excited triplet, with an energy gap of about 4.0 cm^{-1}. The solid-state single-crystal EPR data reveal *g* anisotropy consistent with nitronyl nitroxides. The EPR spectrum in solid methylene chloride shows a half-field transition characteristic of the triplet state. Temperature variation of the intensity of this transition is consistent with a singlet ground state and thermally populated triplet state. Careful examination of the solid-state structure suggests that the observed interaction is not intermolecular because the radical−radical intermolecular contacts are too large. In addition, intramolecular magnetic interactions cannot occur through space because the corresponding distances are greater than 8 Å.

The solution behavior of biradical **1** was investigated by EPR. Room-temperature spectra of biradical **1** in methylene chloride shows a nine-line spectrum with hyperfine coupling to four "equivalent" nitrogen atoms (a_N = 3.8 G). The variation in spectral features with temperature was investigated and displays features typical of alternating line width effects. Such a behavior is characteristic of out-of phase modulation of the hyperfine and exchange interaction parameters due to dynamic behavior in solution. Because the spirocyclic framework is rigid, the dynamic behavior most likely arises from rotation about the radical phenyl carbon−carbon bond. It is suggested that the exchange pathway may be dominated by superexchange through the central spirocyclic carbon, providing the first real evidence for spiroconjugation as a possible pathway for magnetic interaction.

Experimental Section

X-ray Crystal and Molecular Structure Analysis. Data for a blue crystal plate of **1** were collected using Mo Kα radiation (λ = 0.71073 Å), $\theta-2\theta$ scan at 293(2) K on an Enraf-Nonius CAD4 diffractometer. Structure solution and refinement were carried out using the program SHELXS-97. Hydrogen atoms were found from Fourier differences synthesis and refined isotropically. Crystal data: C35H46N4O4, M = 586.76, monoclinic, space group $C2/c$, a = 24.861(10) Å, b = 12.129(3) Å, 12.258(6) Å, α = 90°, β = 117.482(19)°, γ = 90°, V = 3279(2) $Å^3$, Z = 4, d(calc) = 1.189 g cm^{-3}, 3235 reflections collected, final R indices [$I \geq 2\sigma(I)$], 287 parameters, R = 0.0612, wR2 = 0.1243, GOF = 0.984.

EPR and Magnetic Measurements. The single-crystal, powder, and matrix ESR spectra were recorded using a Bruker ESP 300E spectrometer operating at 9.40 GHz. Single-crystal measurements were performed by mounting a single crystal on a sample holder that allowed rotation along the orthogonal axes *x*, *y*, and *z*. Temperatures in the range 4.2−295 K were obtained with an Oxford Instruments ESR9 continuous flow cryostat. Calculation of *g* values was carried out using solid DPPH (g = 2.0034) as a reference. Magnetic susceptibilities of a polycrystalline sample of biradical **1** were measured on a Quantum Design MPMS-5S SQUID magnetometer working down to 2 K and up to 50 kOe.

Synthesis. Materials were purchased from Acros and Aldrich and used without further purification. Methylene chloride was dried and distilled from CaH_2, diethyl ether was dried and distilled from sodium/benzophenone, tributylamine was distilled from NaOH, and acetonitrile was dried and distilled from P_2O_5. Starting spirobiindane bisphenol **3** was synthesized as described in the literature.[26]

a. 6,6′-Ditriflyl-3,3,3′,3′-tetramethyl-1,1′-spirobisindane (4). A solution of 6,6′-dihydroxy-3,3,3′,3′-tetramethyl-1,1′-spirobisindane (**3**; 6.00 g, 19.5 mmol) in anhydrous methylene chloride (90 mL) was treated with anhydrous tributylamine (8.4 g, 45.3 mmol) at 0 °C, and the mixture was stirred for 10 min. Triflic anhydride (12.07 g, 43 mmol) was added, and the reaction mixture was further stirred for 14 h at 25 °C before being quenched by the addition of H_2O (5 mL). The mixture was concentrated in vacuo. Chromatography (SiO_2, methylene chloride) afforded **4** as a colorless solid (9.70 g, 89% yield). ^{1}H NMR ($CDCl_3$, 200 MHz): δ 7.28 (d, 2H, J = 8.3 Hz), 7. 18 (dd, 2H, J = 8.3, 2.3 Hz), 6.65 (d, 2H, J = 2.3 Hz), 2.33 (ABq, 4H, J_{AB} = 11 Hz), 1.45 (s, 6H), 1.39 (s, 6H) ppm. ^{13}C NMR ($CDCl_3$, 50.3 MHz): δ 152.2, 149.2, 123.2, 120.6, 118.6, 116.9, 109.2, 59.1, 57.5, 43.5, 31.4, 29.9 ppm. IR (KBr) ν_{max}: 2963, 2926, 2868, 1482, 1427, 1406, 1212, 1146, 1103, 919, 868, 821, 808, 628, 603, 529, 505 cm^{-1}. Anal. Calcd for $C_{23}H_{22}F_6O_6S_2$: C, 48.25; H, 3.87. Found: C, 48.03; H, 4.02.

b. 6,6′-Dicyano-3,3,3′,3′-tetramethyl-1,1′-spirobisindane (5).[29] A solution of 6,6′-ditriflyl-3,3,3′,3′-tetramethyl-1,1′-spirobisindane (**4**; 0.504 g, 0.88 mmol) in anhydrous acetonitrile (2.5 mL) under inert atmosphere was treated with potassium cyanide (0.254 g, 3.9 mmol), triphenyl phosphine (23 mg, 0.088 mmol), dibromobistriphenylphosphinenickel(II) (33.5 mg, 0.045 mmol), and zinc dust (26.5 mg, 0.40 mmol). The reaction mixture was heated to 60 °C for 3.5 h before being cooled to room temperature and concentrated in vacuo. Chromatography (SiO_2, 20% EtOAc/80% hexane) afforded **5** as a colorless solid (446 mg, 78% yield). ^{1}H NMR ($CDCl_3$, 200 MHz): δ 7.56 (d, 2H, J = 8.0 Hz), 7. 29 (d, 2H, J = 8.0 Hz), 7.04 (s, 2H), 2.32 (ABq, 4H, J_{AB} = 12 Hz), 1.44 (s, 6H), 1.36 (s, 6H) ppm. ^{13}C NMR ($CDCl_3$, 50.3 MHz): δ 156.8, 150.4, 131.6, 128.0, 123.1, 118.9, 111.2, 58.6, 57.5, 44.1, 31.2, 29.6 ppm. IR (KBr) ν_{max}: 2938, 2926, 2866, 2222, 1605, 1485, 1406, 1093, 912, 835 cm^{-1}. Anal. Calcd for $C_{23}H_{22}N_2$: C, 84.63; H, 6.69; N, 8.58. Found: C, 84.31; H, 6.71, N, 8.28.

c. 3,3,3′,3′-Tetramethyl-1,1′-spirobisindane-6,6′-dicarboxaldehyde (6). Through a solution of tin(II) chloride (742 mg, 3.9 mmol) in anhydrous ether (5 mL) was bubbled hydrochloride gas until two phases were apparent. To this solution was added 6,6′-dicyano-3,3,3′,3′-tetramethyl-1,1′-spirobisindane (**5**; 304 mg, 0.93 mmol), and the mixture was stirred for 12 h followed by standing for 21 h. The white solid product was then triturated with anhydrous diethyl ether (3 × 5 mL). To the solid was added H_2O (20 mL), and the solution was heated to 60 °C for 1 h. The aqueous solution was extracted with diethyl ether, washed with saturated NaCl, dried over Na_2SO_4, and concentrated in vacuo. Chromatography (SiO_2, methylene chloride) afforded **6** as a colorless solid (290 mg, 94% yield). ^{1}H NMR ($CDCl_3$, 200 MHz): δ 9.89 (s, 2H), 7.78 (dd, 2H, J = 8.0, 1.0 Hz), 7. 37 (d, 2H, J = 8.0 Hz), 7.31 (d, J = 1.0 Hz), 2.37 (ABq, 4H, J_{AB} = 13 Hz), 1.46 (s, 6H), 1.38 (s, 6H) ppm. IR (KBr) ν_{max}: 2922, 2956, 2853, 1695 cm^{-1}. Anal. Calcd for $C_{23}H_{24}O_2$: C, 83.10; H, 7.28. Found: C, 83.13; H, 7.49.

d. 6,6′-(4,4,5,5-Tetramethylimidazolidine-3-oxide-1-oxyl)-3,3,3′,3′-tetramethyl-1,1′-spirobiindane (1). To a solution of 3,3,3′,3′-tetramethyl-1,1′-spiro biindane-6,6′-dicarboxaldehyde (**6**, 300 mg, 0.90 mmol) in 30 mL of absolute ethanol was added 1,1,2,2-tetramethyl-1,2-dihydroxylaminoethane (269 mg, 1.8 mmol). The solution was

(44) Zheludez, A.; Barone, V.; Bonnet, M.; Delley, B.; Grand, A.; Ressouche, E.; Rey, P.; Subra, R.; Schweizer, J. *J. Am. Chem. Soc.* **1994**, *116*, 2019−2027.

(45) For PhNIT, two independent molecules with differing atomic spin populations were found in the unit cell (see ref 44). The comparison is made with "molecule 2", in which the dihedral angle between nitronyl nitroxide and the phenyl ring, 29.8°, is similar to the value of 28.0° found in our system.

stirred at 30 °C for 45 h, leading to the formation of a white precipitate. The solvent was removed in vacuo, and the resulting solid (crude **7**, 410 mg) was carried to the next step. A solution of 6,6′-(1,3-dihydroxy-4,4,5,5-tetramethyl imidazolidine)-3,3,3′,3′- tetramethyl-1,1′-spirobisindane (**7**, 300 mg, 0.5 mmol) in 20 mL of methanol was treated dropwise with a solution of sodium periodate (10 mg) in methanol (10 mL) until the solution maintained a deep-blue color. Purification by chromatography (SiO_2, 2% methanol, 98% methylene chloride) followed by crystallization from methylene chloride/ether afforded **1** as a blue/black solid (76 mg, 26% yield). IR (KBr) ν_{max}: 2954, 2861, 1352, 1136, 841, 537 cm^{-1}. UV (CH_2Cl_2, λ_{max} in nm, ϵ in parentheses): 232 (7370), 252 (6460), 274 (8580), 350 (4980), 366 (7850), 584 (407), and 614 (500). Anal. Calcd for $C_{23}H_{24}O_2$: C, 83.10; H, 7.28. Found: C, 82.83; H, 7.49.

Acknowledgment. N.L.F. gratefully acknowledges the CNRS for a postdoctoral research fellowship. N.L.F also thanks Prof. P. T Narasimhan for invaluable discussions and Prof. B. Bales for assistance with additional EPR measurements.

Supporting Information Available: Details of X-ray analysis for biradical **1** including tables of atomic coordinates, anisotropic displacement parameters, bond lengths, bond angles, torsions angles, and nonbonding contacts (PDF). CIF data are also available. This material is available free of charge via the Internet at http://pubs.acs.org.

JA993071A